PCCP

Check for updates

CO$_2$ electroreduction on single atom catalysts: the role of the DFT functional†

Debolina Misra,[a] Giovanni Di Liberto [ID] *[b] and Gianfranco Pacchioni [ID] [b]

One key process involving single atom catalysts (SACs) is the electroreduction of CO$_2$ to fuels. The chemistry of SACs differs largely from that of extended catalytic surfaces, presenting an opportunity to improve the ability to activate very stable molecules, such as CO$_2$. In this work, we performed a density functional theory (DFT) study of CO$_2$ activation on a series of SACs, focusing on the role played by the adopted functional in activity predictions. The role of the exchange–correlation functional has been widely investigated in heterogenous catalysts, but it is less explored in SACs. We tested the widely used PBE and the PBE+U corrected functionals against the more robust hybrid PBE0 functional. The results show that PBE is reliable if one is interested in qualitative predictions, but it leads to some inaccuracies in other cases. A possible way to attenuate this effect is by adopting the PBE+U framework, as it gives results that are very similar to PBE0 at an acceptable computational cost. The results of this study further underline the importance of the computational framework adopted in predicting the activity of SACs. The work suggests that one needs to go beyond PBE for quantitative estimates, an important consideration when performing screening and high-throughput calculations.

1. Introduction

The capture of CO$_2$ and its conversion into valuable chemicals, including fuels, is involved in key processes in the ongoing energy transition.[1–4] The conversion of CO$_2$ to fuels would create, in principle, a carbon neutral cycle that can mitigate the impact of the greenhouse effect. The main issue associated with this objective is the strong stability of CO$_2$, which in turn makes its activation hard.[5] The process can be activated by working under harsh conditions with the help of a catalyst.[6–8] The process can be conducted either under thermal or electrochemical conditions, depending on the way energy is supplied.[9,10]

Electrocatalysis offers a viable method for electroreducing CO$_2$ under ambient conditions.[11–13] A significant amount of research is dedicated to the discovery of novel catalytic materials and gaining a fundamental understanding of the physical chemistry behind this reaction. Typical catalytic materials are metal particles,[14–16] based on critical and noble metals.

Single atom catalysis is a relatively new frontier with the potential to reduce the amount of metal loading in catalytic

materials.[17–20] A single atom catalyst (SAC) is made by depositing transition metal atoms with atomic precision on a given support. In addition, metal atom SACs exhibit a specific local coordination that strongly affects their reactivity.[21–24] This characteristic makes SACs analogous to coordination chemistry compounds,[25] as they can form molecular adducts that do not form on conventional extended surfaces.[26–30] This includes not only unconventional reaction intermediates, but also complexes with the solvent, that can compete with the classical reaction intermediates identified on the surface of metal electrodes. If the solvent can also act as a ligand (such as water), it can play a twofold role in SACs, serving both as a solvent and as a ligand. We have recently observed this effect in CO$_2$ electroreduction on a set of SACs supported on nitrogen-doped graphene by means of DFT calculations.[31]

Quantum chemical calculations provide a valuable contribution to the fundamental understanding of the chemistry of SACs.[32,33] Calculations enable access to a SAC with atomistic precision, which would otherwise be difficult to achieve experimentally. It is however important to underline that quantitative predictions can only be made if the simulated model corresponds to the real one. To access this information, it is often mandatory to combine theory with spectroscopy techniques.[34,35]

Besides the quality of the model, the way in which the electronic structure of the system is described plays a primary role.[36] The most widely used methodology for simulating a SAC is DFT, which relies heavily on the parametrization of the

^{a} *Department of Physics, Indian Institute of Information Technology, Design and Manufacturing, Kancheepuram, Chennai 600127, India*

^{b} *Dipartimento di Scienza dei Materiali, Università di Milano – Bicocca, via R. Cozzi 55, Milano 20125, Italy. E-mail: giovanni.diliberto@unimib.it*

† Electronic supplementary information (ESI) available: additional DFT data, supporting figures and tables. See DOI: https://doi.org/10.1039/d4cp00175c

exchange and correlation functional. Although there is an extensive literature dedicated to the assessment of the accuracy and reliability of different functionals on extended catalytic surfaces,[37–41] this aspect is less explored in SACs. The number of screening and high-throughput studies aimed at the discovery of new SACs is increasing steadily, but it largely depends on the standard parametrization of the functional known as generalized gradient approximation (GGA).[33,42–52] However, it is well known that self-interaction error corrected functionals such as the DFT+U approach or hybrid functionals can provide a more accurate description of the chemistry, in particular when transition metals with open shell structures are involved.

In this work, we assessed the accuracy of different DFT functionals in simulating the CO_2 electroreduction on SACs. We tested two popular choices against a reference hybrid functional: the widely adopted PBE functional (GGA),[53] and the PBE+U correction[54] (DFT+U) vs the PBE0 functional (hybrid).[55,56] Previous studies showed that PBE0 can be considered a good benchmark in the framework of DFT.[36] We investigated the role of the functional in (i) the CO_2 activation process, (ii) the nature and stability of the first electrochemical intermediates, and (iii) the competing action of the solvent. CO_2 activation and the first electrochemical step (addition of the first H^+/e^- couple) are two key processes in CO_2 electroreduction. The main purpose of this work is to investigate the effect of the adopted functional on the predictions of the activation of CO_2 on SACs. To address this point, we studied a specific model system, comprising a graphene nanosheet doped with nitrogen exhibiting pyridinic coordination, which is a likely active site, although it is not the only one.[57] Indeed, N-doped graphene is widely adopted as a support for SACs, due to its capability to stably bind metal atoms.[58,59] A distribution of different active sites can be present in real samples. There are basically three most common configurations; a nitrogen atom replacing a carbon one (graphitic defect), four nitrogen atoms having a porphyrin-like arrangement close to a carbon divacancy (pyridinic defect), and a nitrogen atom terminating 5-membered rings instead of the lattice hexagonal ones (pyrrolic defect).[60,61] The catalytic activity may be affected by the local coordination. Some insight into the nature of the species can be evinced from XPS measurements.[62] Also, given the complexity of catalytic pathways leading to fuel formation, in this study

we do not proceed further with the reaction mechanism since we are not focused on a specific product, but rather on assessing the accuracy of the DFT functional for describing CO_2 activation. The results show that the use of PBE leads to significant deviations when compared to PBE0, while the use of PBE+U strongly attenuates the discrepancy. This study suggests that despite PBE being reliable for establishing general trends, it may lead to inaccurate results when trying to be quantitative. This problem can be attenuated by adopting the PBE+U approach.

2. Computational details

The calculations have been performed at the level of density functional theory (DFT) as implemented in the Vienna *Ab Initio* Simulation Package (VASP).[63–65] Simulations were performed including spin polarization and employing the projector-augmented wave (PAW) method.[66,67] The valence electrons were expanded on a set of plane waves with a kinetic cutoff of 400 eV. The dispersion interactions were included using Grimme's D3 correction.[68] The reciprocal space was sampled in order to provide converged results. A $5 \times 5 \times 1$ Monkhorst–Pack grid was adopted.[69] The convergence criteria for the electronic and ionic loops were set at 10^{-6} eV and 10^{-3} eV Å^{-1} respectively. In the case of PBE+U, the U values for TM were taken from the literature. These values have been discussed for SACs, tested and benchmarked elsewhere (see Table S1, ESI†).[70,71]

We fully optimized a 4×4 supercell of graphene, with $a = b = 9.87$ Å and $\gamma = 120°$.[72,73] This was used to build the 4N-Gr support, where a 15 Å-thick vacuum layer was included along the non-periodic direction to avoid interaction between the periodic replicas of the system. A C-divacancy was created in the cell, and four C atoms were replaced with N atoms to build the 4N-Gr (pyridine) support. The TM atom was embedded into the coordination site resulting in the TM@4N-Gr structure.[30,74,75] Fig. 1 shows the prototype structure of the SACs and the investigated TM atoms.

In each case, the atomic coordinates have been fully relaxed. The approximation of keeping the lattice vectors frozen at those of graphene implies a negligible error, less than 0.1 eV,[70] and therefore it can be considered acceptable for the purpose of the
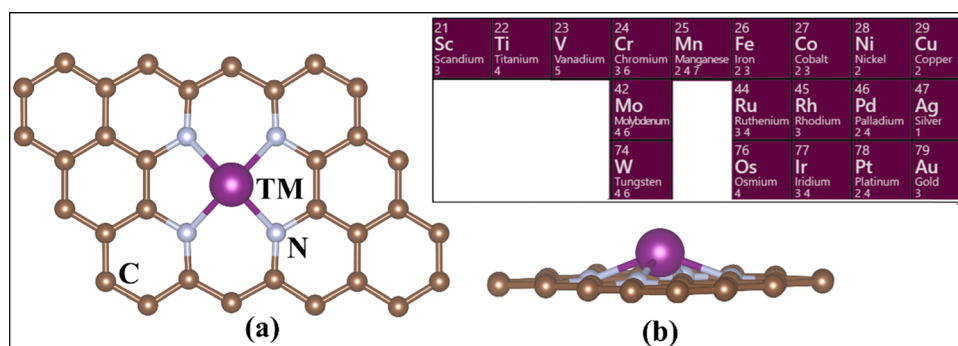

Fig. 1 (a) Top view and (b) side view of the TM-embedded N-doped graphene structure. The inset shows the TM considered in this study.

This journal is © the Owner Societies 2024

Phys. Chem. Chem. Phys., 2024, **26**, 10746–10756 | **10747**

study. The adhesion energies and magnetization of the TMs are reported in Table S1 (ESI†). When adsorbed in the cavity, the metal atom can either remain in the same plane as the C atoms or it can protrude from the surface layer. Fig. S1 (ESI†) shows the structure of two representative cases, namely, Mo@4N-Gr and Ni@4N-Gr.

The adsorption energy (ΔE_{ads}) of an adsorbed species on the TM@4N-Gr SAC is calculated as:

$$\Delta E_{ads} = E_{SAC+mol} - E_{SAC} - E_{mol} \qquad (1)$$

where $E_{SAC+mol}$, E_{SAC} and E_{mol} are the energies of the catalyst with the molecule adsorbed, of the bare catalyst and of the molecule, respectively. In this work we neglect any reaction barrier different from those arising from thermochemistry, following the approach proposed by Norskov and co-workers.[76] This implies assuming that some correlation exists between the thermodynamic energies of the reaction steps and the corresponding activation energy. Since the specific purpose of this study is not to provide absolute predictions, but to show the effect of the adopted functional on the activation of CO_2 on SACs, we can consider this approximation acceptable. The reaction Gibbs free energy of each reaction step was obtained by using Norskov's Computational Hydrogen Electrode (CHE) approach,[77–79]

$$\Delta G = \Delta E_{ads} - T\Delta S + \Delta E_{zpe} \qquad (2)$$

where ΔE_{zpe} and ΔS are the changes in zero-point energy and entropy, respectively. The values of ZPE and entropic contributions for CO_2 and H_2O gas phase molecules and the reaction intermediates were taken from the literature[80] and NIST database, respectively. The entropies of solid-state species were neglected.[78] A way to overcome this approximation is to estimate the vibrational entropy of solids by means of the partition function formalism working in a harmonic fashion. If one neglects this contribution, the expected error is about 0.1–0.2 eV, which can be considered acceptable given the specific purpose of the study. It should be mentioned, however, that if one aims at reproducing the experimental complexity, this effect should be accounted for, together with many other effects such as solvation, applied voltage and pH.[81–85] Further details and working equations are reported in the ESI.†

3. Results

As mentioned before, we investigated the performance of three popular DFT exchange–correlation functionals. The first is the PBE functional,[53] one of the most popular for the study of SACs. It is known that this functional may lead to some inaccuracies when compared to high level benchmark calculations,[36,75] mainly because it tends to over delocalize electrons in a system. However, given its efficiency, it is widely used for screening and predictive studies.[33,44,45,86–89] One approach to overcome the issues with PBE is to employ hybrid functionals, *i.e.*, including a given fraction of exact Fock exchange into the functional.[90–92] A popular choice is the PBE0 parametrization.[55,56] A previous work by Patel *et al.* demonstrated that PBE0 shows negligible differences from high level CCSD(T) calculations of a SAC used as a test case.[36] Therefore, PBE0 can be considered a solid benchmark for other functionals. Hybrid functionals are however rather expensive when associated with plane wave approaches. A compromise between accuracy and computational cost is represented by the DFT+U approach.[54] In this framework one adds an *ad hoc* correction term mimicking the effect of the exact Fock exchange in hybrid functionals. The extra computational cost is negligible with respect to PBE, but the choice of the U correction term is delicate.

3.1. Benchmarking PBE and PBE+U against PBE0

We start by benchmarking the reliability of PBE and PBE+U against the PBE0 hybrid functional in the activation of CO_2, eqn (3a).

$$CO_2 + * \rightarrow *CO_2 \qquad (3a)$$
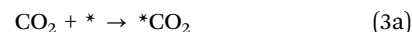
As reported elsewhere,[31] at the PBE level only few SACs are able to effectively chemisorb CO_2, resulting in bending of the O–C–O angle. In particular, Sc, Ti, Mo, Ru, W, and Os@4N-Gr bind and activate CO_2. In the other cases (among those showed in Fig. 1) CO_2 remains physisorbed to the SAC. To assess the performance of PBE and PBE+U against PBE0, we focus on the SACs that activate CO_2. For comparison, we also included a representative SAC that is not able to activate the molecule, Ni@4N-Gr. Then, we simulated the formation of the reaction intermediates resulting from the addition of the first H+ and e− couple on the SACs. CO_2 reduction can occur *via* formation of *COOH (eqn (3b)) or *OCHO (eqn (3c)) intermediates.[93–96]

Table 1 Reaction energies, E_{ads}, and reaction free energies, ΔG, of adsorbed CO_2 and reaction intermediates formed on TM@4N-Gr, obtained with PBE0, PBE+U and PBE approaches. Values are in eV

	PBE0						PBE+U						PBE					
	*CO_2		*COOH		*OCHO		*CO_2		*COOH		*OCHO		*CO_2		*COOH		*OCHO	
TM	E_{ads}	ΔG	E_{ads}	ΔG	E_{ads}	ΔG	E_{ads}	ΔG	E_{ads}	ΔG	E_{ads}	ΔG	E_{ads}	ΔG	E_{ads}	ΔG	E_{ads}	ΔG
Sc	−1.01	−0.33	−1.72	−0.69	−3.39	−2.38	−0.92	−0.24	−1.47	−0.44	−3.14	−2.13	−0.84	−0.16	−1.38	−0.35	−3.01	−2
Ti	−1.39	−0.71	−1.66	−0.63	−2.84	−1.83	−1.31	−0.63	−1.41	−0.38	−2.78	−1.77	−1.58	−0.9	−1.57	−0.54	−2.61	−1.61
Ni	0.02	0.70	—	—	1.12	2.13	−0.13	0.56	1.03	2.06	0.86	1.87	−0.13	0.55	1.04	2.07	0.78	1.79
Mo	−0.84	−0.16	−0.37	0.66	−1.75	−0.74	−0.73	−0.05	−0.59	0.44	−1.84	−0.83	−1.41	−0.73	−1.45	−0.41	−2.21	−1.2
Ru	0.38	1.06	−0.77	0.26	−0.09	0.92	0.16	0.84	−0.64	0.39	0.07	1.08	−0.11	0.57	−0.99	0.04	−0.16	0.85
W	−1.56	−0.88	−1.15	−0.12	−2.5	−1.49	−1.65	−0.97	−1.27	−0.24	−2.47	−1.46	−1.92	−1.24	−1.96	−0.92	−2.6	−1.59
Os	−0.47	0.21	−1.17	−0.14	−0.69	0.33	−0.45	0.23	−1.01	0.02	−0.65	0.36	−0.74	−0.06	−1.12	−0.09	−0.71	0.3

10748 | *Phys. Chem. Chem. Phys.*, 2024, **26**, 10746–10756

This journal is © the Owner Societies 2024

$$CO_2 + H^+ + e^- \, * \rightarrow \, *COOH \qquad (3b)$$

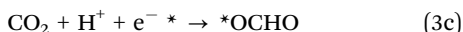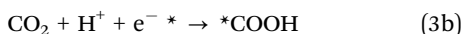$$CO_2 + H^+ + e^- \, * \rightarrow \, *OCHO \qquad (3c)$$

Table 1 presents the reaction energies, reaction free energies and structural geometries related to $*CO_2$, $*COOH$, and $*OCHO$ adsorbed species on TM@4N-Gr obtained using PBE, PBE+U, and PBE0 approaches (* indicates the site where an adsorbed

molecular fragment is bound). In the case of $*COOH$ adsorption on Ni@4N-Gr with PBE0 we encountered unsurmountable convergence issues, and therefore we are not reporting any value in Table 1. Reaction free energies reported in Table 1 are calculated according to eqn (3a)–(3c) and refer to the adsorption of reaction intermediates to the SACs.

PBE offers large deviations from PBE0, with a mean absolute error (MAE) of 0.30 eV, 0.43 eV, and 0.23 eV for $*CO_2$, $*COOH$, and $*OCHO$, respectively. The maximum deviation is very high, being 0.57 eV, 1.08 eV, and 0.46 eV for $*CO_2$, $*COOH$, and $*OCHO$ respectively. This result already shows the problems connected with the use of the PBE functional: in the adsorption of CO_2 the differences can be up to 0.6 eV and for the formation of the intermediates, they can be even larger, exceeding 1 eV in some cases, Table 1 and Fig. 2. PBE+U provides estimates closer to PBE0, as the MAE is 0.11 eV, 0.19 eV, and 0.13 eV for $*CO_2$, $*COOH$, and $*OCHO$, respectively. Similarly, the maximum deviation is nearly the same in all the cases, 0.22 eV ($*CO_2$), 0.25 eV ($*COOH$), and 0.26 eV ($*OCHO$), Fig. 2. Thus, the energy computed at the PBE+U level is very similar to that obtained at the PBE0 level, with a MAE always lower than 0.2 eV and a maximum deviation always smaller than 0.3 eV. This shows that PBE+U is sufficiently reliable for providing quantitative estimates of the reaction energetics at an acceptable computational cost. These results are in line with previous findings showing that PBE+U estimates of H atom adsorption on TM@4N-Gr SACs closely match with the PBE0 ones (MAE less than 0.2 eV).[75]

3.2. CO_2 activation

The results show that PBE+U provides results that closely resemble those obtained with the benchmark PBE0 functional. Therefore, in the following, discussion is restricted to the comparison of PBE and PBE+U results.

We concentrate first on the activation of CO_2 on the full set of 19 SACs, Fig. 1. Fig. 3 shows representative cases of CO_2
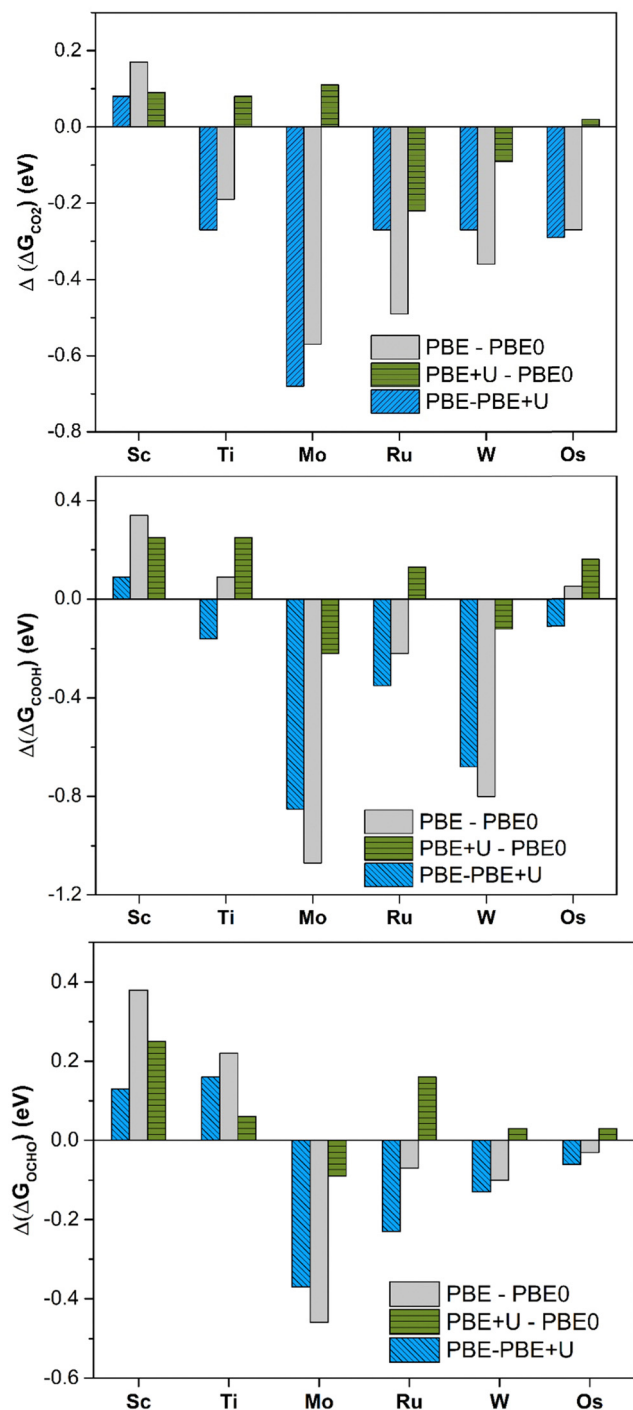

Fig. 2 Deviation of Gibbs free energies comparing different levels of theory for $*CO_2$, $*COOH$, and $*OCHO$ adsorption on TM@4N-Gr.
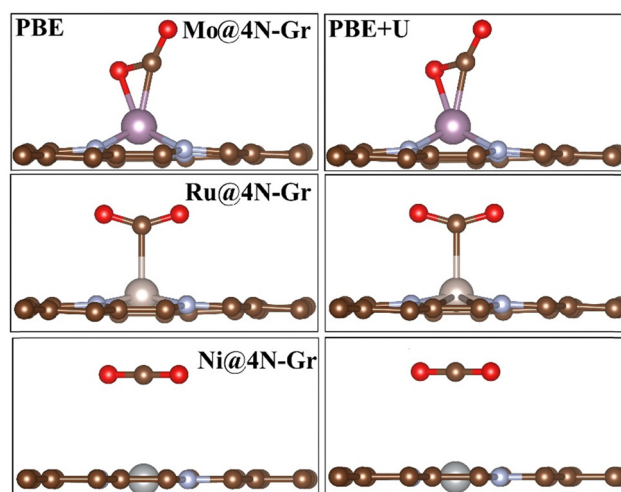

Fig. 3 CO_2 adsorption on TM@4N-Gr: chemisorption *versus* physisorption. Left: PBE; right: PBE+U.

This journal is © the Owner Societies 2024

Phys. Chem. Chem. Phys., 2024, **26**, 10746–10756 | **10749**

Table 2 Reaction free energies and structural parameters for CO_2 adsorption on TM@4N-Gr with PBE and PBE+U approaches. In bold cases where CO_2 is chemically adsorbed to the SAC[a]

TM	PBE				PBE+U			
	E_{ads} (eV)	ΔG (eV)	<O–C–O	TM–C (Å)	E_{ads} (eV)	ΔG (eV)	<O–C–O	TM–C (Å)
Sc	**−0.84**	**−0.16**	**139**	**2.42**	**−0.92**	**−0.24**	**139.48**	**2.44**
Ti	**−1.58**	**−0.90**	**133**	**2.05**	**−1.31**	**−0.63**	**133.73**	**2.06**
V	−0.08	0.60	177	3.19	−0.07	0.61	178.53	3.23
Cr	−0.11	0.57	179	3.40	−0.10	0.58	179.7	3.40
Mn	−0.10	0.58	180	3.44	−0.09	0.59	179.7	3.45
Fe	−0.10	0.58	180	3.32	−0.09	0.59	179.94	3.32
Co	0.93	1.61	180	3.24	−0.11	0.57	179.06	3.29
Ni	−0.13	0.55	179	3.24	−0.13	0.56	179.09	3.26
Cu	0.04	0.72	180	3.31	−0.10	0.58	179.86	3.32
Mo	**−1.41**	**−0.73**	**131**	**2.03**	**−0.73**	**−0.05**	**132.70**	**2.04**
Ru	**−0.11**	**0.57**	**147**	**2.16**	**0.16**	**0.84**	**148.60**	**2.20**
Rh	−0.18	0.50	176	3.22	−0.15	0.53	177.85	2.30
Pd	−0.13	0.55	179	3.32	−0.13	0.55	178.95	3.32
Ag	−0.17	0.51	179	4.20	−0.37	0.31	178.73	4.22
W	**−1.92**	**−1.24**	**129**	**2.02**	**−1.65**	**−0.97**	**130.75**	**2.06**
Os	**−0.74**	**−0.06**	**139**	**2.02**	**−0.45**	**0.23**	**140.14**	**2.02**
Ir	−0.19	0.49	176	3.28	−0.16	0.52	177.60	3.34
Pt	−0.14	0.54	178	3.35	−0.14	0.54	178.45	3.35
Au	−0.12	0.56	180	3.44	−0.12	0.56	179.83	3.44

[a] MAE of PBE with respect to PBE+U: MAE chemisorption 0.41 eV; MAE physisorption 0.04 eV.

adsorption. The CO_2 molecule can be attached to the SAC by means of TM–O and TM–C interactions (Mo@4N-Gr), or through a TM–C bond (Ru@4N-Gr). In the first case, the complex shows bidentate bonding, while in the latter case the interaction occurs only *via* the C atom of the CO_2 molecule. In the case of physisorption, the CO_2 molecule is distant from the SAC (~3.0 Å). Fig. S2 (ESI†) shows the structure of *CO_2 adsorbed on various SACs. Table 2 presents the calculated adsorption energy, Gibbs free energies of *CO_2 and structural parameters.

The number of SACs capable of activating CO_2 remains unchanged when adopting the PBE+U approach, indicating that PBE is sufficiently reliable for obtaining qualitative predictions. The picture changes when looking at quantitative estimates. In fact, on average, the PBE values deviate by 0.41 eV from the PBE+U ones, with cases where the difference reaches 1 eV (Co@4N-Gr), see Fig. 4. Not surprisingly, PBE+U

impacts the results only when CO_2 is chemisorbed. If one restricts to the physisorption cases, the MAE is 0.04 eV, Fig. 4.

3.3. Reaction intermediates

After discussing the activation of CO_2, we now move to the reaction intermediates arising from the addition of the first H+ and e− couple to CO_2, the first step in CO_2 electroreduction. Fig. S3 (ESI†) shows the structure of *COOH and *OCHO molecular fragments adsorbed on the SACs considered.

When comparing the stability of the *COOH intermediate at PBE and PBE+U levels of theory, we see that the MAE is still high, 0.32 eV, comparable to that of CO_2 activation (0.41 eV), Table 3. Even the maximum deviation is large, 0.86 eV (Mo@4N-Gr), close to 1 eV, as found before. Besides Mo@4N-Gr, two other systems are critical, namely, Ru@4N-Gr and W@4N-Gr, with a deviation equal to 0.35 eV and 0.69 eV, respectively. This implies that the stability of reaction intermediates is very sensitive to the adopted functional and the usage of PBE can lead to significant errors.
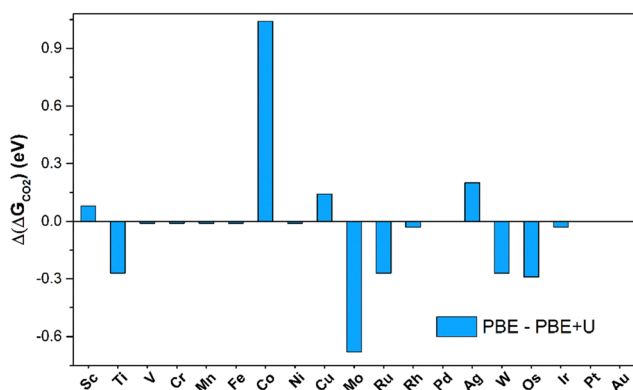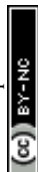

Fig. 4 Deviation of Gibbs free energies computed at PBE and PBE+U levels for CO_2 adsorption on TM@4N-Gr.

Table 3 Reaction energies, E_{ads}, and reaction free energies, ΔG, for reaction intermediates on TM@4N-Gr obtained with PBE and PBE+U approaches. Values are in eV

TM	PBE				PBE+U			
	*COOH		*OCHO		*COOH		*OCHO	
	E_{ads}	ΔG	E_{ads}	ΔG	E_{ads}	ΔG	E_{ads}	ΔG
Sc	−1.38	−0.35	−3.01	−2.00	−1.47	−0.44	−3.14	−2.13
Ti	−1.57	−0.54	−2.61	−1.61	−1.41	−0.38	−2.78	−1.77
Ni	1.04	2.07	0.78	1.79	1.03	2.06	0.86	1.87
Mo	−1.45	−0.41	−2.21	−1.20	−0.59	0.44	−1.84	−0.83
Ru	−0.99	0.04	−0.16	0.85	−0.64	0.39	0.07	1.08
W	−1.96	−0.92	−2.60	−1.59	−1.27	−0.24	−2.47	−1.46
Os	−1.12	−0.09	−0.71	0.30	−1.01	0.02	−0.65	0.36

Table 4 Reaction energies, reaction free energies and structural parameters for H_2O adsorption on TM@4N-Gr, with PBE and PBE+U approaches

TM	PBE				PBE+U			
	E_{ads} (eV)	ΔG (eV)	<H–O–H	$d_{TM–O}$ (Å)	E_{ads} (eV)	ΔG (eV)	<H–O–H	$d_{TM–O}$ (Å)
Sc	−1.00	−0.42	107	2.30	−1.05	−0.47	107	2.30
Ti	−0.97	−0.39	106	2.20	−0.91	−0.33	106	2.20
Ni	−0.14	0.44	103	3.31	−0.14	0.44	103	3.26
Mo	−0.63	−0.05	105	2.30	−0.49	0.09	105	2.30
Ru	−0.25	0.33	105	2.70	−0.29	0.29	105	2.70
W	−0.73	−0.15	106	2.30	−0.74	−0.16	106	2.30
Os	−0.06	0.52	105	2.80	−0.25	0.33	105	2.80

The stability of OCHO* seems to be less sensitive to the functional adopted, since the MAE is 0.17 eV and the maximum deviation is 0.37 eV only, Table 3. Regarding CO_2 adsorption, PBE is still reliable in providing qualitative predictions, since the relative stability of the two intermediates remains unchanged. In particular, with both PBE and PBE+U, OCHO* is more stable than COOH* on Sc, Ti, Ni, Mo, and W@4N-Gr, while COOH* is more stable on Ru and Os@4N-Gr.

3.4. Competing action of water

In this section, we analyze the impact of the exchange–correlation functional on another relevant point for the study of the electrochemical reduction of CO_2 with SACs: the role of water. In electrochemical reactions, a fundamental role is played by the solvent, water. An appropriate way to account for it requires a dynamic approach that explicitly considers the catalyst/water interface. Interestingly, we have recently reported that on SACs, water does not only act as a solvent in the reaction but can also act as a ligand competing with CO_2 and the other reaction intermediates in binding to the TM center.[31] In this respect, this finding is another demonstration of the similarity between SACs and organometallic compounds. Here we discuss the effect of the adopted functional on the prediction of the "coordination" effect played by water. A dedicated study is planned to address the complex problem of solvation.

We first adsorbed a water molecule on the SACs considered in this work, as shown in Table 4, where the calculated Gibbs free energies at PBE and PBE+U levels are reported along with the relevant structural information. If one considers the structure of the complex, negligible changes are found between the two functionals, as shown in Fig. 5 where the representative case of Mo@4N-Gr is shown.

The analysis of the energetics suggests that in this case PBE provides acceptable results, since the MAE is less than 0.1 eV (0.07 eV) and the maximum deviation is 0.19 eV only, Fig. 6.
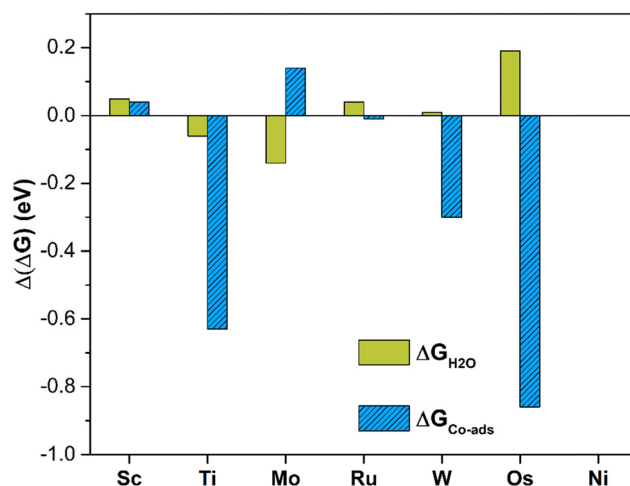
Fig. 6 Deviation of Gibbs free energies computed at PBE and PBE+U levels for H_2O adsorption (green) and CO_2 co-adsorption (blue) in the presence of *H_2O on TM@4N-Gr.

Comparing the Gibbs free energy of *CO_2 and *H_2O to that of SACs, one can evince that the two ligands have comparable interactions with the TM center and in fact compete for bonding to it. A comparison of the Gibbs free energies of adsorption is reported in Tables 2 and 4. On Sc, Ni, and Ru@4N-Gr, water adsorption is more favorable than CO_2 adsorption. In the latter case, *H_2O is more stable by 0.55 eV than *CO_2, Tables 2 and 4. Of course, this is a simplified model since here the nature of liquid water is not considered. Other approaches should be adopted in order to properly describe the catalyst/water interface including bulk water and explicit solvation spheres.[82,97–101]

Finally, we considered the adsorption of CO_2 in the presence of *H_2O. Here we assume that the adsorption occurs on the opposite side. Further work in the future will be dedicated to the exploration of the several possible co-adsorption
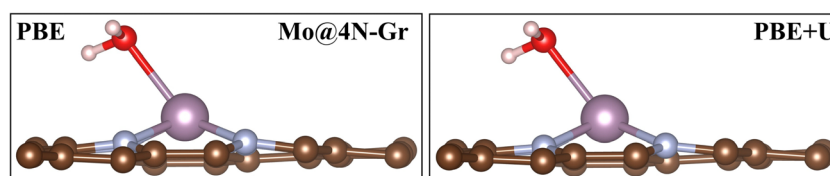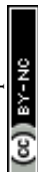

Fig. 5 H_2O adsorption on Mo@4N-Gr with PBE and PBE+U methods.

This journal is © the Owner Societies 2024

Phys. Chem. Chem. Phys., 2024, **26**, 10746–10756 | **10751**

Table 5 Reaction energies, E_{ads}, and reaction free energies, ΔG, for CO_2 and H_2O co-adsorption on TM@4N-Gr, using PBE and PBE+U functionals. Values in eV

TM	PBE		PBE+U	
	E_{ads}	ΔG	E_{ads}	ΔG
Sc	−0.08	0.60	−0.12	0.56
Ti	−0.79	−0.11	−0.16	0.52
Ni	−0.14	0.54	−0.14	0.54
Mo	0.39	1.07	0.25	0.93
Ru	−0.15	0.53	−0.14	0.54
W	−1.37	−0.69	−1.07	−0.39
Os	−0.36	−0.32	−0.14	0.54

configurations. The adsorption energy is calculated as follows.

$$E_{ads}^{CO_2} = E_{SAC+CO_2+H_2O} - E_{SAC+H_2O} - E_{CO_2} \qquad (4)$$

Table 5 presents the calculated Gibbs free energies. Fig. S5 (ESI†) shows the structure of *CO_2 in the presence of *H_2O on the various SACs. Even in this case PBE and PBE+U provide similar results, with a MAE of 0.19 eV, but with relevant exceptions. In fact, in the case of Ti@4N-Gr, PBE and PBE+U differ by 0.63 eV, Fig. 6. This value largely contributes to the MAE, as MAE decreases to 0.11 eV by excluding Ti@4N-Gr. It this respect, the adoption of PBE+U in place of PBE looks more solid.

4. Conclusions

In this work we performed a computational study of the initial phases of CO_2 electroreduction on single atom catalysts consisting of TM atoms stabilized in nitrogen-doped graphene. We simulated the bonding and activation of CO_2 as well as the first hydrogenation step leading to the formation of *COOH and *OCHO intermediates, as they usually represent the most complex steps to overcome. The focus is on the role of the exchange–correlation functional used to simulate CO_2 activation and reduction on SACs. Previous studies have demonstrated that the PBE functional, one of the most commonly used functionals for this kind of calculation, is sufficiently reliable when looking at trends and general rules, while it may fail in providing quantitative estimates. The picture can be improved by invoking the PBE+U approach, or even better hybrid functionals, such as the PBE0 functional that we used as a benchmark. The results of this study show that PBE+U reproduces the PBE0 results with satisfactory accuracy, at a much lower computational cost. Both PBE+U and PBE0 provide more reliable results than the standard PBE functional. In particular, for CO_2 adsorption, PBE estimates deviate on average by 0.3 eV from PBE0 ones, while the maximum deviation can reach up to 0.5 eV. The effect can be tamed by invoking PBE+U as the MAE decreases to 0.1 eV. The picture is similar when looking at *COOH and *OHCH intermediates, as the deviation between PBE and PBE0 is 0.43 eV and 0.23 eV, respectively, with a maximum deviation of up to one eV. The difference between PBE0 and PBE+U is much lower, 0.19 eV and 0.13 eV. Therefore, PBE+U is an acceptable compromise

between accuracy and computational cost. Despite the important quantitative effect on the reaction energies, PBE looks sufficiently reliable when looking at qualitative trends, such as the energetic ordering of stability of *COOH and *OCHO intermediates, which remains unchanged when the self-interaction correction is introduced.

Finally, we investigated the competing effects of water adsorption and CO_2 binding to the active site. We first considered simple water adsorption, finding that the discrepancy between PBE and PBE+U is small, as shown by a MAE of 0.07 eV, and a maximum deviation of 0.19 eV. Next, we considered co-adsorption on the same site of water and CO_2. Here the MAE between PBE and PBE+U becomes more relevant, 0.19 eV.

In general, the work serves as another example highlighting the importance of moving beyond the PBE functional when trying to provide quantitative predictions of the catalytic activity of SACs. In fact, while PBE looks sufficiently reliable for a preliminary screening of the catalytic activity, significant differences arise when the system is treated with the more rigorous PBE+U or even better PBE0 functionals. This level of theory becomes essential when one is interested in determining the reaction profile and the expected activity of a potential new catalyst.

Further work will be dedicated to searching for correlations between thermodynamic and activation energies, aiming to provide insight to verify if the universal relations discovered for extended catalysts are valid also in the context of SACs.

Author contributions

D. M. performed the calculations and analysis. G. D. L. and G. P. supervised the project. G. D. L. wrote the first draft. All authors contributed to designing the study, analyzing the results, and preparing the final draft.

Data availability

The data reported in this article can be found in the cited literature and can be requested from the authors upon reasonable inquiry.

Conflicts of interest

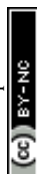There are no conflicts to declare.

Acknowledgements

References

1 G. Centi and J. Čejka, Needs and Gaps for Catalysis in Addressing Transitions in Chemistry and Energy from a Sustainability Perspective, *ChemSusChem*, 2019, **12**, 621–632.

2 C. Gürsan and V. de Gooyert, The systemic impact of a transition fuel: Does natural gas help or hinder the energy transition?, *Renewable Sustainable Energy Rev.*, 2021, **138**, 110552.

3 W. A. Smith, T. Burdyny, D. A. Vermaas and H. Geerlings, Pathways to Industrial-Scale Fuel Out of Thin Air from CO_2 Electrolysis, *Joule*, 2019, **3**, 1822–1834.

4 H. C. Lau, S. Ramakrishna, K. Zhang and A. V. Radhamani, The Role of Carbon Capture and Storage in the Energy Transition, *Energy Fuels*, 2021, **35**, 7364–7386.

5 X. Chang, T. Wang and J. Gong, CO_2 photo-reduction: insights into CO_2 activation and reaction on surfaces of photocatalysts, *Energy Environ. Sci.*, 2016, **9**, 2177–2196.

6 A. Álvarez, M. Borges, J. J. Corral-Pérez, J. G. Olcina, L. Hu, D. Cornu, R. Huang, D. Stoian and A. Urakawa, CO_2 Activation over Catalytic Surfaces, *Chem. Phys. Chem.*, 2017, **18**, 3135–3141.

7 H.-J. Son, C. Pac and S. O. Kang, Inorganometallic Photocatalyst for CO_2 Reduction, *Acc. Chem. Res.*, 2021, **54**, 4530–4544.

8 S. Fang, M. Rahaman, J. Bharti, E. Reisner, M. Robert, G. A. Ozin and Y. H. Hu, Photocatalytic CO_2 reduction, *Nat. Rev. Methods Primers*, 2023, **3**, 61.

9 S. Xie, W. Zhang, X. Lan and H. Lin, CO_2 Reduction to Methanol in the Liquid Phase: A Review, *ChemSusChem*, 2020, **13**, 6141–6159.

10 P. Saha, S. Amanullah and A. Dey, Selectivity in Electrochemical CO_2 Reduction, *Acc. Chem. Res.*, 2022, **55**, 134–144.

11 A. Senocrate and C. Battaglia, Electrochemical CO_2 reduction at room temperature: Status and perspectives, *J. Energy Storage*, 2021, **36**, 102373.

12 X. Duan, J. Xu, Z. Wei, J. Ma, S. Guo, S. Wang, H. Liu and S. Dou, Metal-Free Carbon Materials for CO_2 Electrochemical Reduction, *Adv. Mater.*, 2017, **29**, 1701784.

13 M. Bevilacqua, J. Filippi, H. A. Miller and F. Vizza, Recent Technological Progress in CO_2 Electroreduction to Fuels and Energy Carriers in Aqueous Environments, *Energy Technol.*, 2015, **3**, 197–210.

14 A. A. Peterson and J. K. Nørskov, Activity Descriptors for CO_2 Electroreduction to Methane on Transition-Metal Catalysts, *J. Phys. Chem. Lett.*, 2012, **3**, 251–258.

15 M. C. O. Monteiro, F. Dattila, B. Hagedoorn, R. García-Muelas, N. López and M. T. M. Koper, Absence of CO_2 electroreduction on copper, gold and silver electrodes without metal cations in solution, *Nat. Catal.*, 2021, **4**, 654–662.

16 F. Dattila, R. R. Seemakurthi, Y. Zhou and N. López, Modeling Operando Electrochemical CO_2 Reduction, *Chem. Rev.*, 2022, **122**, 11085–11130.

17 S. K. Kaiser, Z. Chen, D. Faust Akl, S. Mitchell and J. Pérez-Ramírez, Single-Atom Catalysts across the Periodic Table, *Chem. Rev.*, 2020, **120**, 11703–11809.

18 H.-Y. Zhuo, X. Zhang, J.-X. Liang, Q. Yu, H. Xiao and J. Li, Theoretical Understandings of Graphene-based Metal Single-Atom Catalysts: Stability and Catalytic Performance, *Chem. Rev.*, 2020, **120**, 12315–12341.

19 A. Wang, J. Li and T. Zhang, Heterogeneous single-atom catalysis, *Nat. Rev. Chem.*, 2018, **2**, 65–81.

20 M. A. Bajada, J. Sanjosé-Orduna, G. Di Liberto, S. Tosoni, G. Pacchioni, T. Noël and G. Vilé, Interfacing single-atom catalysis with continuous-flow organic electrosynthesis, *Chem. Soc. Rev.*, 2022, **51**, 3898–3925.

21 N. Sathishkumar and H.-T. Chen, Regulating the Coordination Environment of Single-Atom Catalysts Anchored on Thiophene Linked Porphyrin for an Efficient Nitrogen Reduction Reaction, *ACS Appl. Mater. Interfaces*, 2023, **15**, 15545–15560.

22 X. Li, Q. Zhou, S. Wang, Y. Li, Y. Liu, Q. Gao and Q. Wu, Tuning the Coordination Environment to Effect the Electrocatalytic Behavior of a Single-Atom Catalyst toward the Nitrogen Reduction Reaction, *J. Phys. Chem. C*, 2021, **125**, 11963–11974.

23 H. Xu, Y. Zhao, Q. Wang, G. He and H. Chen, Supports promote single-atom catalysts toward advanced electrocatalysis, *Coord. Chem. Rev.*, 2022, **451**, 214261.

24 G. Di Liberto, L. A. Cipriano and G. Pacchioni, Single Atom Catalysts: What Matters Most, the Active Site or The Surrounding?, *ChemCatChem*, 2022, **14**, e202200611.

25 M. K. Samantaray, V. D'Elia, E. Pump, L. Falivene, M. Harb, S. Ould Chikh, L. Cavallo and J.-M. Basset, The Comparison between Single Atom Catalysis and Surface Organometallic Catalysis, *Chem. Rev.*, 2020, **120**, 734–813.

26 G. Di Liberto and G. Pacchioni, Modeling Single-Atom Catalysis, *Adv. Mater.*, 2023, **35**, 2307150.

27 G. Di Liberto, L. A. Cipriano and G. Pacchioni, Role of Dihydride and Dihydrogen Complexes in Hydrogen Evolution Reaction on Single-Atom Catalysts, *J. Am. Chem. Soc.*, 2021, **143**, 20431–20441.

28 L. Zhong and S. Li, Unconventional Oxygen Reduction Reaction Mechanism and Scaling Relation on Single-Atom Catalysts, *ACS Catal.*, 2020, **10**, 4313–4318.

29 L. A. Cipriano, G. Di Liberto and G. Pacchioni, Superoxo and Peroxo Complexes on Single-Atom Catalysts: Impact on the Oxygen Evolution Reaction, *ACS Catal.*, 2022, 11682–11691.

30 I. Barlocco, L. A. Cipriano, G. Di Liberto and G. Pacchioni, Does the Oxygen Evolution Reaction follow the classical OH*, O*, OOH* path on single atom catalysts?, *J. Catal.*, 2023, **417**, 351–359.

This journal is © the Owner Societies 2024

Phys. Chem. Chem. Phys., 2024, **26**, 10746–10756 | **10753**

31 D. Misra, G. Di Liberto and G. Pacchioni, CO_2 electrore-duction on single atom catalysts: Is water just a solvent?, *J. Catal.*, 2023, **422**, 1–11.

32 S. Tosoni, G. Di Liberto, I. Matanovic and G. Pacchioni, Modelling single atom catalysts for water splitting and fuel cells: A tutorial review, *J. Power Sources*, 2023, **556**, 232492.

33 Z. Chen, J. Zhao, C. R. Cabrera and Z. Chen, Computational Screening of Efficient Single-Atom Catalysts Based on Graphitic Carbon Nitride (g-C_3N_4) for Nitrogen Electro-reduction, *Small Methods*, 2019, **3**, 1800368.

34 G. Di Liberto, S. Tosoni, L. A. Cipriano and G. Pacchioni, A Few Questions about Single-Atom Catalysts: When Modeling Helps, *Acc. Mater. Res.*, 2022, **3**, 986–995.

35 F. Kraushofer and G. S. Parkinson, Single-Atom Catalysis: Insights from Model Systems, *Chem. Rev.*, 2022, **122**, 14911–14939.

36 A. M. Patel, S. Ringe, S. Siahrostami, M. Bajdich, J. K. Nørskov and A. R. Kulkarni, Theoretical Approaches to Describing the Oxygen Reduction Reaction Activity of Single-Atom Catalysts, *J. Phys. Chem. C*, 2018, **122**, 29307–29318.

37 A. J. Garza and G. E. Scuseria, Predicting Band Gaps with Hybrid Density Functionals, *J. Phys. Chem. Lett.*, 2016, **7**, 4165–4170.

38 G. Pacchioni, Modeling doped and defective oxides in catalysis with density functional theory methods: Room for improvements, *J. Chem. Phys.*, 2008, **28**, 182505.

39 P. Janthon, S. (Andy) Luo, S. M. Kozlov, F. Viñes, J. Limtrakul, D. G. Truhlar and F. Illas, Bulk Properties of Transition Metals: A Challenge for the Design of Universal Density Functionals, *J. Chem. Theory Comput.*, 2014, **10**, 3832–3839.

40 K. C. Ko, O. Lamiel-García, J. Y. Lee and F. Illas, Performance of a modified hybrid functional in the simultaneous description of stoichiometric and reduced TiO_2 polymorphs, *Phys. Chem. Chem. Phys.*, 2016, **18**, 12357–12367.

41 P. Janthon, S. (Andy) Luo, S. M. Kozlov, F. Viñes, J. Limtrakul, D. G. Truhlar and F. Illas, Bulk Properties of Transition Metals: A Challenge for the Design of Universal Density Functionals, *J. Chem. Theory Comput.*, 2014, **10**, 3832–3839.

42 L. Xu, L.-M. Yang and E. Ganz, Mn–graphene single-atom catalyst evaluated for CO oxidation by computational screening, *Theor. Chem. Acc.*, 2018, **137**, 1–13.

43 H. Niu, X. Wang, C. Shao, Z. Zhang and Y. Guo, Computational Screening Single-Atom Catalysts Supported on g-CN for N2 Reduction: High Activity and Selectivity, *ACS Sustainable Chem. Eng.*, 2020, **8**, 13749–13758.

44 M. Umer, S. Umer, M. Zafari, M. Ha, R. Anand, A. Hajibabaei, A. Abbas, G. Lee and K. S. Kim, Machine learning assisted high-throughput screening of transition metal single atom based superb hydrogen evolution electrocatalysts, *J. Mater. Chem. A*, 2022, **10**, 6679–6689.

45 Y. Zhou, G. Gao, J. Kang, W. Chu and L.-W. Wang, Computational screening of transition-metal single atom doped C 9 N 4 monolayers as efficient electrocatalysts for water splitting, *Nanoscale*, 2019, **11**, 18169–18175.

46 X. Zhai, L. Li, X. Liu, Y. Li, J. Yang, D. Yang, J. Zhang, H. Yan and G. Ge, A DFT screening of single transition atoms supported on MoS_2 as highly efficient electrocatalysts for the nitrogen reduction reaction, *Nanoscale*, 2020, **12**, 10035–10043.

47 Z. Wang, J. Zhao, Q. Cai and F. Li, Computational screening for high-activity MoS_2 monolayer-based catalysts for the oxygen reduction reaction via substitutional doping with transition metal, *J. Mater. Chem. A*, 2017, **5**, 9842–9851.

48 V. Fung, G. Hu, Z. Wu and D. Jiang, Descriptors for Hydrogen Evolution on Single Atom Catalysts in Nitrogen-Doped Graphene, *J. Phys. Chem. C*, 2020, **124**, 19571–19578.

49 H.-C. Huang, Y. Zhao, J. Wang, J. Li, J. Chen, Q. Fu, Y.-X. Bu and S.-B. Cheng, Rational design of an efficient descriptor for single-atom catalysts in the hydrogen evolution reaction, *J. Mater. Chem. A*, 2020, **8**, 9202–9208.

50 S. Agarwal, R. Kumar, R. Arya and A. K. Singh, Rational Design of Single-Atom Catalysts for Enhanced Electrocatalytic Nitrogen Reduction Reaction, *J. Phys. Chem. C*, 2021, **125**, 12585–12593.

51 M. D. Hossain, Z. Liu, M. Zhuang, X. Yan, G.-L. Xu, C. A. Gadre, A. Tyagi, I. H. Abidi, C.-J. Sun, H. Wong, A. Guda, Y. Hao, X. Pan, K. Amine and Z. Luo, Rational Design of Graphene-Supported Single Atom Catalysts for Hydrogen Evolution Reaction, *Adv. Energy Mater.*, 2019, **9**, 1803689.

52 L. Wu, T. Guo and T. Li, Rational design of transition metal single-atom electrocatalysts: a simulation-based, machine learning-accelerated study, *J. Mater. Chem. A*, 2020, **8**, 19290–19299.

53 J. P. Perdew, K. Burke and M. Ernzerhof, Generalized Gradient Approximation Made Simple, *Phys. Rev. Lett.*, 1996, **77**, 3865–3868.

54 S. L. Dudarev, G. A. Botton, S. Y. Savrasov, C. J. Humphreys and A. P. Sutton, Electron-energy-loss spectra and the structural stability of nickel oxide: An LSDA + U study, *Phys. Rev. B: Condens. Matter Mater. Phys.*, 1998, **57**, 1505–1509.

55 C. Adamo and V. Barone, Toward reliable density functional methods without adjustable parameters: The PBE0 model, *J. Chem. Phys.*, 1999, **110**, 6158–6170.

56 J. P. Perdew, M. Ernzerhof and K. Burke, Rationale for mixing exact exchange with density functional approximations, *J. Chem. Phys.*, 1996, **105**, 9982–9985.

57 B. Singh, M. B. Gawande, A. D. Kute, R. S. Varma, P. Fornasiero, P. McNeice, R. V. Jagadeesh, M. Beller and R. Zbořil, Single-Atom (Iron-Based) Catalysts: Synthesis and Applications, *Chem. Rev.*, 2021, **121**, 13620–13697.

58 H. Fei, J. Dong, D. Chen, T. Hu, X. Duan, I. Shakir, Y. Huang and X. Duan, Single atom electrocatalysts supported on graphene or graphene-like carbons, *Chem. Soc. Rev.*, 2019, **48**, 5207–5241.

59 C. Rivera-Cárcamo and P. Serp, Single Atom Catalysts on Carbon-Based Materials, *ChemCatChem*, 2018, **10**, 5058–5091.

10754 | *Phys. Chem. Chem. Phys.*, 2024, **26**, 10746–10756

This journal is © the Owner Societies 2024
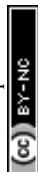
60 Y. Wang, Y. Shao, D. W. Matson, J. Li and Y. Lin, Nitrogen-Doped Graphene and Its Application in Electrochemical Biosensing, *ACS Nano*, 2010, **4**, 1790–1798.

61 X.-F. Li, K.-Y. Lian, L. Liu, Y. Wu, Q. Qiu, J. Jiang, M. Deng and Y. Luo, Unraveling the formation mechanism of graphitic nitrogen-doping in thermally treated graphene with ammonia, *Sci. Rep.*, 2016, **6**, 23495.

62 V. Dao, L. A. Cipriano, S.-W. Ki, S. Yadav, W. Wang, G. Di Liberto, K. Chen, H. Son, J.-K. Yang, G. Pacchioni and I.-H. Lee, 2D/2D Z-scheme-based α-Fe$_2$O$_3$ @NGr heterojunction implanted with Pt single-atoms for remarkable photocatalytic hydrogen evolution, *Appl. Catal., B*, 2023, **330**, 122586.

63 G. Kresse and J. Hafner, Ab initio molecular-dynamics simulation of the liquid-metal–amorphous-semiconductor transition in germanium, *Phys. Rev. B: Condens. Matter Mater. Phys.*, 1994, **49**, 14251–14269.

64 G. Kresse and J. Furthmüller, Efficiency of ab-initio total energy calculations for metals and semiconductors using a plane-wave basis set, *Comput. Mater. Sci.*, 1996, **6**, 15–50.

65 G. Kresse and J. Hafner, Ab initio molecular dynamics for liquid metals, *Phys. Rev. B: Condens. Matter Mater. Phys.*, 1993, **47**, 558–561.

66 P. E. Blöchl, Projector augmented-wave method, *Phys. Rev. B: Condens. Matter Mater. Phys.*, 1994, **50**, 17953–17979.

67 G. Kresse and D. Joubert, From ultrasoft pseudopotentials to the projector augmented-wave method, *Phys. Rev. B: Condens. Matter Mater. Phys.*, 1999, **59**, 1758–1775.

68 S. Grimme, J. Antony, S. Ehrlich and H. Krieg, A consistent and accurate ab initio parametrization of density functional dispersion correction (DFT-D) for the 94 elements H-Pu, *J. Chem. Phys.*, 2010, **132**, 154104.

69 H. J. Monkhorst and J. D. Pack, Special points for Brillouin-zone integrations, *Phys. Rev. B: Solid State*, 1976, **13**, 5188–5192.

70 G. Di Liberto, L. A. Cipriano and G. Pacchioni, Universal Principles for the Rational Design of Single Atom Electrocatalysts? Handle with Care, *ACS Catal.*, 2022, 5846–5856.

71 I. Barlocco, G. Di Liberto and G. Pacchioni, Hydrogen and oxygen evolution reactions on single atom catalysts stabilized by a covalent organic framework, *Energy Adv.*, 2023, **2**, 1022–1029.

72 D. Van Dao, L. A. Cipriano, G. Di Liberto, T. T. D. Nguyen, S.-W. Ki, H. Son, G.-C. Kim, K. H. Lee, J.-K. Yang, Y.-T. Yu, G. Pacchioni and I.-H. Lee, Plasmonic Au nanoclusters dispersed in nitrogen-doped graphene as a robust photocatalyst for light-to-hydrogen conversion, *J. Mater. Chem. A*, 2021, **9**, 22810–22819.

73 D. Van Dao, G. Di Liberto, H. Ko, J. Park, W. Wang, D. Shin, H. Son, Q. Van Le, T. Van Nguyen, V. Van Tan, G. Pacchioni and I.-H. Lee, LaFeO$_3$ meets nitrogen-doped graphene functionalized with ultralow Pt loading in an impactful Z-scheme platform for photocatalytic hydrogen evolution, *J. Mater. Chem. A*, 2022, **10**, 3330–3340.

74 I. Barlocco, G. Di Liberto and G. Pacchioni, New scaling relationships for the oxygen evolution reaction on single atom catalysts, *Catal. Today*, 2024, **427**, 114409.

75 I. Barlocco, L. A. Cipriano, G. Di Liberto and G. Pacchioni, Modeling Hydrogen and Oxygen Evolution Reactions on Single Atom Catalysts with Density Functional Theory: Role of the Functional, *Adv. Theory Simul.*, 2022, 2200513.

76 J. K. Nørskov, T. Bligaard, A. Logadottir, S. Bahn, L. B. Hansen, M. Bollinger, H. Bengaard, B. Hammer, Z. Sljivancanin, M. Mavrikakis, Y. Xu, S. Dahl and C. J. H. Jacobsen, Universality in Heterogeneous Catalysis, *J. Catal.*, 2002, **209**, 275–278.

77 J. K. Nørskov, T. Bligaard, A. Logadottir, J. R. Kitchin, J. G. Chen, S. Pandelov and U. Stimming, Trends in the Exchange Current for Hydrogen Evolution, *J. Electrochem. Soc.*, 2005, **152**, J23.

78 J. K. Nørskov, J. Rossmeisl, A. Logadottir, L. Lindqvist, J. R. Kitchin, T. Bligaard and H. Jónsson, Origin of the Overpotential for Oxygen Reduction at a Fuel-Cell Cathode, *J. Phys. Chem. B*, 2004, **108**, 17886–17892.

79 J. K. Nørskov, T. Bligaard, J. Rossmeisl and C. H. Christensen, Towards the computational design of solid catalysts, *Nat. Chem.*, 2009, **1**, 37–46.

80 Y. Yang, J. Li, C. Zhang, Z. Yang, P. Sun, S. Liu and Q. Cao, Theoretical Insights into Nitrogen-Doped Graphene-Supported Fe, Co, and Ni as Single-Atom Catalysts for CO$_2$ Reduction Reaction, *J. Phys. Chem. C*, 2022, **126**, 4338–4346.

81 J. A. Gauthier, C. F. Dickens, L. D. Chen, A. D. Doyle and J. K. Nørskov, Solvation Effects for Oxygen Evolution Reaction Catalysis on IrO$_2$ (110), *J. Phys. Chem. C*, 2017, **121**, 11455–11463.

82 G. Di Liberto, G. Pacchioni, Y. Shao-Horn and L. Giordano, Role of Water Solvation on the Key Intermediates Catalyzing Oxygen Evolution on RuO$_2$, *J. Phys. Chem. C*, 2023, **127**, 10127–10133.

83 S. Rojas-Carbonell, K. Artyushkova, A. Serov, C. Santoro, I. Matanovic and P. Atanassov, Effect of pH on the Activity of Platinum Group Metal-Free Catalysts in Oxygen Reduction Reaction, *ACS Catal.*, 2018, **8**, 3041–3053.

84 A. Goyal and M. T. M. Koper, The Interrelated Effect of Cations and Electrolyte pH on the Hydrogen Evolution Reaction on Gold Electrodes in Alkaline Media, *Angew. Chem., Int. Ed.*, 2021, **60**, 13452–13462.

85 T. Cheng, L. Wang, B. V. Merinov and W. A. Goddard, Explanation of Dramatic pH-Dependence of Hydrogen Binding on Noble Metal Electrode: Greatly Weakened Water Adsorption at High pH, *J. Am. Chem. Soc.*, 2018, **140**, 7787–7790.

86 J. Wang, Z. Zhang, Y. Li, Y. Qu, Y. Li, W. Li and M. Zhao, Screening of Transition-Metal Single-Atom Catalysts Anchored on Covalent–Organic Frameworks for Efficient Nitrogen Fixation, *ACS Appl. Mater. Interfaces*, 2022, **14**, 1024–1033.

87 X. Zhai, L. Li, X. Liu, Y. Li, J. Yang, D. Yang, J. Zhang, H. Yan and G. Ge, A DFT screening of single transition

This journal is © the Owner Societies 2024

Phys. Chem. Chem. Phys., 2024, **26**, 10746–10756 | **10755**

atoms supported on MoS₂ as highly efficient electrocatalysts for the nitrogen reduction reaction, *Nanoscale*, 2020, **12**, 10035–10043.

88 C. Ling, Y. Ouyang, Q. Li, X. Bai, X. Mao, A. Du and J. Wang, A General Two-Step Strategy–Based High-Throughput Screening of Single Atom Catalysts for Nitrogen Fixation, *Small Methods*, 2019, **3**, 1800376.

89 M. Zafari, D. Kumar, M. Umer and K. S. Kim, Machine learning-based high throughput screening for nitrogen fixation on boron-doped single atom catalysts, *J. Mater. Chem. A*, 2020, **8**, 5209–5216.

90 A. D. Becke, Density-functional exchange-energy approximation with correct asymptotic behavior, *Phys. Rev. A: At., Mol., Opt. Phys.*, 1988, **38**, 3098–3100.

91 A. D. Becke, A new mixing of Hartree–Fock and local density-functional theories, *J. Chem. Phys.*, 1993, **98**, 1372–1377.

92 A. D. Becke, Density-functional thermochemistry. III. The role of exact exchange, *J. Chem. Phys.*, 1993, **98**, 5648–5652.

93 R. Kortlever, J. Shen, K. J. P. Schouten, F. Calle-Vallejo and M. T. M. Koper, Catalysts and Reaction Pathways for the Electrochemical Reduction of Carbon Dioxide, *J. Phys. Chem. Lett.*, 2015, **6**, 4073–4082.

94 P. Huang, M. Cheng, H. Zhang, M. Zuo, C. Xiao and Y. Xie, Single Mo atom realized enhanced CO₂ electro-reduction into formate on N-doped graphene, *Nano Energy*, 2019, **61**, 428–434.

95 P. Lozano-Reis, H. Prats, P. Gamallo, F. Illas and R. Sayós, Multiscale Study of the Mechanism of Catalytic CO₂ Hydrogenation: Role of the Ni(111) Facets, *ACS Catal.*, 2020, **10**, 8077–8089.

96 A. Jurado, Á. Morales-García, F. Viñes and F. Illas, Molecular Mechanism and Microkinetic Analysis of the Reverse Water Gas Shift Reaction Heterogeneously Catalyzed by the Mo 2 C MXene, *ACS Catal.*, 2022, **12**, 15658–15667.

97 N. Daelman, M. Capdevila-Cortada and N. López, Dynamic charge and oxidation state of Pt/CeO₂ single-atom catalysts, *Nat. Mater.*, 2019, **18**, 1215–1221.

98 G. Di Liberto and L. Giordano, Role of solvation model on the stability of oxygenates on Pt(111): A comparison between microsolvation, extended bilayer, and extended metal/water interface, *Electrochem. Sci. Adv.*, 2024, **4**, e2100204.

99 G. Di Liberto, R. Conte and M. Ceotto, ''Divide-and-conquer'' semiclassical molecular dynamics: An application to water clusters, *J. Chem. Phys.*, 2018, **148**, 104302.

100 P. Gono, F. Ambrosio and A. Pasquarello, Effect of the Solvent on the Oxygen Evolution Reaction at the TiO₂–Water Interface, *J. Phys. Chem. C*, 2019, **123**, 18467–18474.

101 A. Bouzid, P. Gono and A. Pasquarello, Reaction pathway of oxygen evolution on Pt(1 1 1) revealed through constant Fermi level molecular dynamics, *J. Catal.*, 2019, **375**, 135–139.

10756 | *Phys. Chem. Chem. Phys.*, 2024, **26**, 10746–10756

This journal is © the Owner Societies 2024